RESEARCH ARTICLE

*National Science Open*
3: 20230071, 2024
https://doi.org/10.1360/nso/20230071

Engineering

Special Topic: Energy Systems of Low Carbon Buildings

# pH-sensitive tunable thermochromic hydrogel with carbon quantum dots for smart windows

Sai Zhong[1,#], Yuxuan Xue[1,#], Kuanwen Wang[1], Haoyang Li[3], Yanghua Lu[3], Zhenqian Pang[2,3], Tengyao Jiang[1,*] & Gang Tan[2,3,*]

[1]*School of Environmental Science and Engineering, Nanjing Tech University, Nanjing 211816, China;*
[2]*College of Civil Engineering and Architecture, Zhejiang University, Hangzhou 310058, China;*
[3]*The Smart Materials for Architecture Research Lab, Innovation Center of Yangtze River Delta, Zhejiang University, Jiaxing 314100, China*

#Contributed equally to this work.
*Corresponding authors (emails: jiangty@njtech.edu.cn (Tengyao Jiang); tangang@zju.edu.cn (Gang Tan))

Received 1 November 2023; Revised 7 February 2024; Accepted 7 March 2024; Published online 12 March 2024

**Abstract:** Thermoresponsive hydrogels have been designed for smart windows to dynamically modulate solar radiation, but their inherent drawbacks of long response time and imperfectly matched phase transition temperature have limited their wide applications. This work reports a novel composite hydrogel consisting of hydroxypropyl cellulose, polyacrylic acid, and carbon quantum dots with intriguing features of tunable transition temperature and enhanced switching speed. The composite hydrogel demonstrated flexible tunability in transition temperature by controlling the hydrogen ion concentration and a fast response speed by dopping with carbon dots for efficient photothermal conversion. The building energy simulation was carried out to investigate the impacts of transition temperature variations and solar regulations on the space cooling/heating loads under different climate conditions, revealing the necessity of tunability of both transition temperature and solar transmittance in thermochromic smart windows. This novel design of thermochromic composite hydrogel provides insight into theoretical and experimental support for future adaptive building envelopes.

**Keywords:** thermochromic hydrogel, transition temperature, carbon quantum dots, lower critical solution temperature tunability, building energy efficiency

## INTRODUCTION

As the population grows and social development progresses, the demand for buildings is increasing. This is accompanied by a sharp increase in building energy consumption and great pressure on the ecological environment [1,2]. The global building sector consumes 30% of total energy and contributes 28% of the world's carbon emissions [3]. In China, the current use of building energy accounts for about 21% of the nation's total energy consumption. It is hypothesized that the annual compound growth rate of building energy usage will be 2.9% in the next 30 years with the rapid advancement of urbanization and the deep adjustment of industrial structure [4]. In order to achieve the goal of reducing greenhouse gas emissions, accelerating the pace of decarburization in the construction and building industry has become an urgent issue

in China [5,6].

In particular, about 50% of total energy in the building sector is consumed for heating, ventilation, and air conditioning. Transparent building envelopes such as windows control the sunlight transmittance and ensure human visual comfort and health. However, compared with other building envelope structures, transparent components possess the most sensitive and active heat exchange [7] and are considered the least energy-efficient component, contributing to at least 20% of the energy loss in buildings [8,9]. Current energy-saving glass techniques, such as multi-layer insulating glass, low-e coating, thermal reflective coating, and aerogel interlayer, are capable of reducing the building energy consumption; however, the most developed glazing systems generally have static physical property [10,11] without the capability of dynamic optical feature to adapt various ambient environments across the world in regard of time and space. A frontier concept of smart building is therefore proposed that requires adaptive/smart building envelopes in response to the dynamic human needs or environmental conditions.

The adaptive smart window structure with unique dynamic light-thermal regulation properties brings innovative solutions to this problem [12,13], which can adjust its optical properties in a reversible manner in response to external stimuli such as electricity, light, and heat. Thermochromic (TC) material is one of the most advanced materials that can respond to temperature changes by automatically adjusting solar energy transmission without any additional energy input [14–16]. To date, $VO_2$ is the most widely studied TC material for smart window applications, while its development faces challenges of low solar modulation ($\Delta T_{sol} < 20\%$), high phase transition temperature ($T_c \sim 68°C$), and mono-functionality [17,18]. As many researchers considered, ideal TC smart window materials typically require high solar modulation ($\Delta T_{so} \sim 50\%$) and a phase transition temperature close to room temperature ($T_c \sim 26°C$) [19,20]. Recently, the temperature-responsive hydrogel polymers with amphiphilic features that can spontaneously and reversibly change the solubility state have gained massive attention [21]. When the temperature is lower than the lower critical solution temperature (LCST), the polymer is hydrophilic and completely miscible with water; when the temperature is higher than LCST, its hydrophobicity increases, and the polymer shrinks in volume, discharging the water slowly [22]. PNIPAm-based hydrogel is a typical TC material as it presents a highly transparent state at a temperature lower than 32°C and gradually transforms to translucent or opaque with the increase in temperature [23]. However, the complicated preparation process and low mechanical strength at high solubility have limited its further development. Hydroxypropyl cellulose (HPC) hydrogels with hydrophilic hydroxyl groups and hydrophobic epoxy ether backbone can be employed as an alternative TC material for smart windows. Due to its feature of nontoxic and biocompatible, the HPC material is frequently used for medical purposes such as artificial tears, lubricant for artificial eyes, and medicine binder [24]. With superior properties of easy preparation and being derived from biomass [25,26], it shows scalable-producing potential as functional layers in smart windows. Whereas the LCST of HPC hydrogel ($T_c \sim 42°C$) is higher than the temperature required for building applications in the design of thermochromic smart windows [27]. Yang *et al*. [28] reported that the addition of NaCl could reduce the LCST of HPC hydrogels, and found that the LCST dropped from 42°C to 30°C when NaCl addition increased from 0.5% to 5%. However, HPC undergoes an extraction reaction during the introduction of inorganic salts (e.g., NaCl). Previous studies have revealed that HPC can be crosslinked with other polymers, such as acrylic acid (AA) and polyacrylic acid (PAA), by hydrogen bonding, and therefore the LCST was more sensitive to the solution's pH level [29–32]. This phenomenon can be explained by the fact that the adjustment to the pH level results in a change of the

interaction (e.g., hydrogen bonding forces) between the hydrogel chains and the solvent molecules (e.g., water in hydrogel-based smart window), thus influencing the hydrophilicity and hydrophobicity of the hydrogels.

However, TC materials normally require a period of time for sunlight radiating exposure to heat up and trigger the phase transition, which may take as long as 10 min or even longer [12]. From this point of view, TC materials' response time is tremendously longer than that of electrochromic materials, which is commonly about seconds to a minute. A so-called hysteresis process becomes one of the important factors affecting the energy-saving effect of thermochromic smart windows. The Warwick team [33] found that reducing the lag gradient in phase transition process and lowering the phase transition temperature can increase the energy efficiency of smart windows by up to 51%. Meanwhile, slow response speed will introduce uneven heating to hydrogel materials and result in non-uniform and discomfort vision to indoor occupants. Incorporation of nanoparticles with photothermal conversion, such as precious metals [34], semiconductors [35], and organic conjugated polymers [36], can provide required heat to quickly trigger the phase transition of smart window. Carbon dots (CDs) demonstrate excellent photothermal effects arising from intriguing quantum confinement in a zero-dimensional (0D) scale and have the ability to efficiently absorb light energy and convert it into heat [37,38]. The CDs are capable as photothermal active sites that strongly absorb light in a broad range of solar wavelength window with a high light-to-heat conversion efficiency, and thus can be used for remarkable applications in the fields of photothermal therapy [39], seawater desalination [40,41], etc. In addition, CDs have advantages of low cost, easy to prepare, and stable water dispersion compared with inorganic nanoparticle counterparts. These characteristics grant CDs massive attention in the field of thermochromic hydrogel smart window [42–44], performed as matrix fillers to accelerate the switching speed.

In this work, a novel composite hydrogel from HPC and PAA for thermochromic smart window application has been designed and fabricated, demonstrating tunable phase transition temperature. The thermal response rate of the hydrogel has also been improved by dopping with photothermal CDs. The microstructure and optical properties of the newly developed TC material have been experimentally characterized. Finally, the energy performance of the smart window installed with this tunable TC material has been simulated using EnergyPlus software.

## MATERIALS AND METHODS

### Preparation of the HPC-PAA/CDs composite hydrogel

HPC ($M_W$ = 100,000, Aladdin Co. Ltd., China) and PAA ($M_W$ = 3000, Aladdin Co. Ltd., China) were mixed with deionized water until the solids were completely dissolved. A certain amount of CDs (dispersed in organic solvents with granularity of 2–5 nm, Jiangsu Xianfeng Nanomaterial Technology Co., Ltd., China) with a concentration of 1 mg/L was slowly added into the solution by stirring. Diluted HCl and NaOH solutions (Sigma-Aldrich, USA) at a concentration of 1 mol/L were pre-prepared and applied to control the pH value of the above-mixed solution. Then the mixture solution was sonicated at an oscillation power of 500 W. The oscillation time was set to 8 min, and the oscillation interval was set to 5 s. After completion, the HPC-PAA/CDs composite hydrogel was aged to remove bubbles, and finally, the transparent hydrogel was

obtained.

### Construction of the HPC-PAA composite hydrogel smart window

Two transparent glass slides with a size of 60 mm × 60 mm × 1 mm (Lianyungang Dongxu Quartz Products Factory, China) were sealed with 3 M sealant to prevent leakage of the hydrogel solution, and the thickness of the gap was 0.6 mm. As shown in Figure 1, the prepared HPC-PAA composite hydrogel was then injected into the gap between the double glass panels. Then, the top edge of the glass pane was sealed using 3 M sealant to form the HPC-PAA composite hydrogel smart window device with a sandwich structure.

### Material characterization

The microscopic morphology of the sample was determined by scanning electron microscopy (SEM, Hitachi Regulus 8100, Japan) at an operating voltage of 5 kV. The cooled (room temperature (RT)) and heated (50°C) hydrogel solutions were frozen using liquid nitrogen, followed by the vacuum drying process to remove the solvents. The freeze-dried hydrogel samples were characterized by Fourier transform infrared spectroscopy (FTIR, Nicolet iS20, USA) to determine the potential interaction between HPC and PAA organic compounds in the HPC-PAA hybrid hydrogel. The scanning step rate was set at 4 $cm^{-1}$ and the scanning range was 400–4000 $cm^{-1}$. The optical properties of the composite hydrogel smart window device were obtained using ultraviolet-visible near-infrared spectrometer (UV-Vis-NIR, UV-3600i Plus, Japan) in the spectral wavelength range of 300–2500 nm with a scan rate of 10 nm/s. The spectrophotometer was equipped with a heating plate using a heating rate of 0.5°C/min.

### Building energy consumption calculation

In order to evaluate the effect of the tunable phase transition temperature of the HPC-PAA composite hydrogel smart window on energy saving, a simplified single-room model was constructed and utilized for building energy simulation using EnergyPlus. EnergyPlus is a professional software developed by the Department of Energy (DOE), US, which is widely used to conduct whole-building energy simulation [45–49]. The physical specifications of the smart window, such as solar transmittance and reflectivity as well as thermal and dimensional parameters, were imported into the EnergyPlus model, and thus the monthly and annual energy consumptions were obtained. Five cities with different climate types, Nanjing, Singapore, Beijing, Moscow, and Helsinki, were selected to investigate and compare the effect of the tunable transition temperature on energy performance.

## RESULTS

### Characterization of the hydrogel sample

Figure 1A presents a sketched preparation process for the HPC-PAA composite hydrogel and subsequent assembly of the smart window sandwich device through material dissolution, centrifugal mixing, injection,

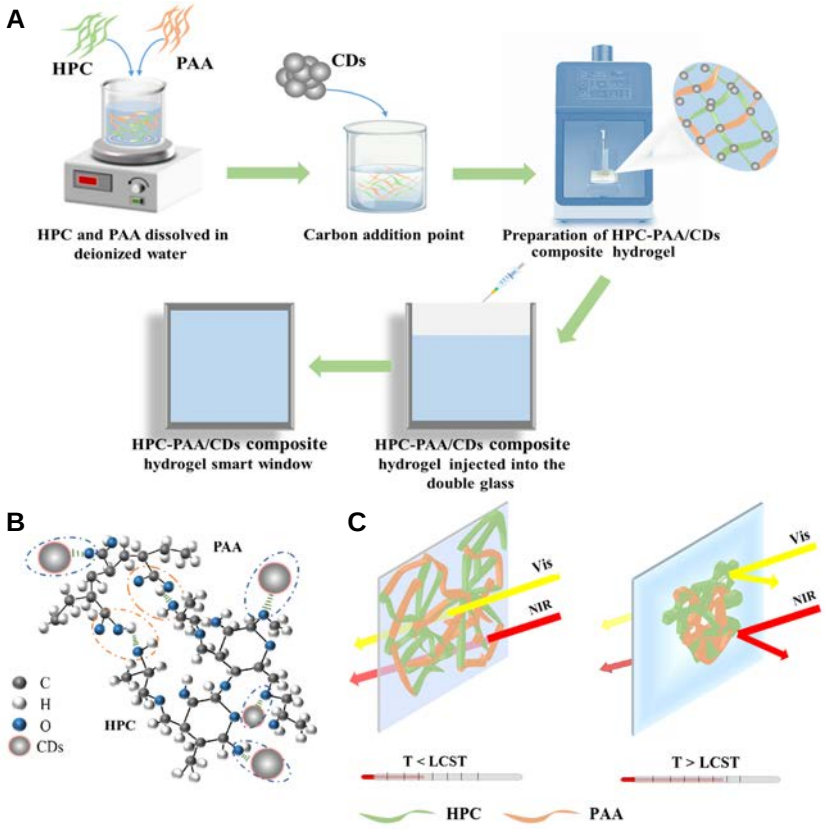


**Figure 1** (A) Preparation flow chart of HPC-PAA composite hydrogel; (B) graph of interactions between the hydrogel components; (C) solar modulation of HPC-PAA composite hydrogel before and after phase transition.

and sealing. As shown in Figure 1B, these two components of HPC and PAA were forming rigid 3D network structures by hydrogen bonds and chain entanglements so that the LCST point can be controlled by adjusting the hydrogen ion concentrations in the system. The hydrogen ion works as a type of hydrogen bonding donor and destroys the interactions between hydrogel chains and solvent molecules, thus modulating the hydrophilicity of the hydrogel, as well as its LCST value. Hence, when the temperature is around the LCST, an obvious phase transition of the hydrogel from hydrophilic-dominant swollen state to hydrophobic-dominant collapse state would initiate, resulting in a reduced solar radiation transmission, including both visible light and near-infrared regions (Figure 1C).

Figure 2 illustrates the microscopy images of the as-synthesized hydrogel samples. The microstructures of pure HPC, HPC-PAA, and HPC-PAA/CDs composite hydrogel powder samples after water removal by freeze-drying at 25 and 50°C are compared, demonstrating the micellar morphology of hydrogel before and after phase transition. It can be observed from Figure 2A that the pure HPC hydrogel sample at 25°C mainly possessed a flake fiber structure with irregular distribution. When the sample was heated to 50°C, some of the flaky fibers were curled into a granular shape from a swollen state (Figure 2D). In contrast, HPC-PAA composite hydrogel samples were crosslinked mainly in a needle-like fiber network at 25°C, forming uniform pore structures with a diameter of about 10 μm (Figure 2B), which was likely due to the formation of a cross-linked network structure of HPC and PAA through hydrogen bonding. After the phase transition, the

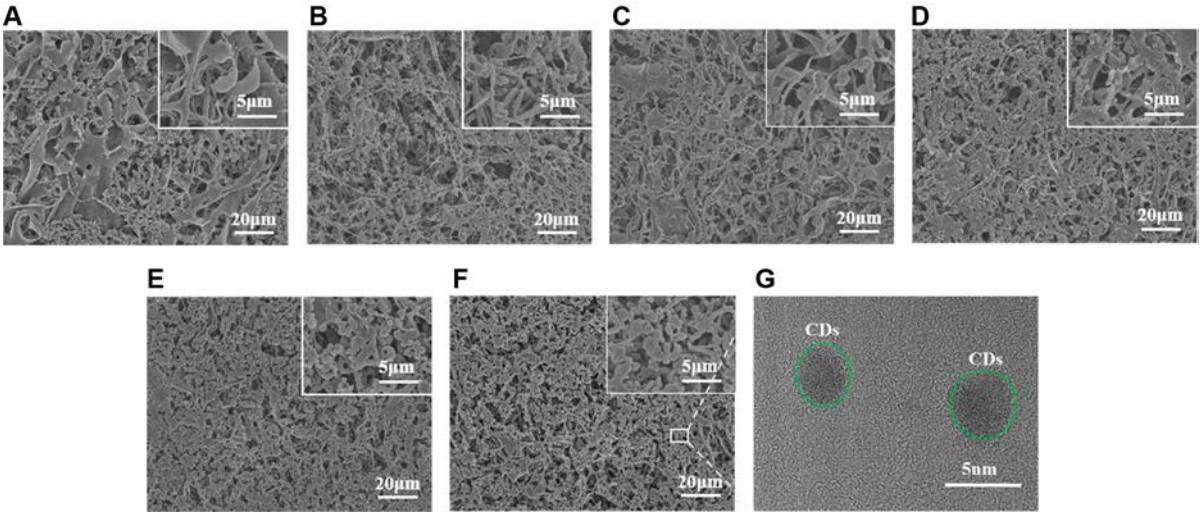


**Figure 2** SEM images of pure HPC hydrogel powder, HPC-PAA composite hydrogel powder and HPC-PAA/CDs composite hydrogel powder: (A) HPC, 25°C; (B) HPC-PAA, 25°C; (C) HPC-PAA/CDs, 25°C; (D) HPC, 50°C; (E) HPC-PAA, 50°C; (F) HPC-PAA/CDs, 50°C. (G) TEM image of the HPC-PAA/CD composite hydrogel sample at 50°C.

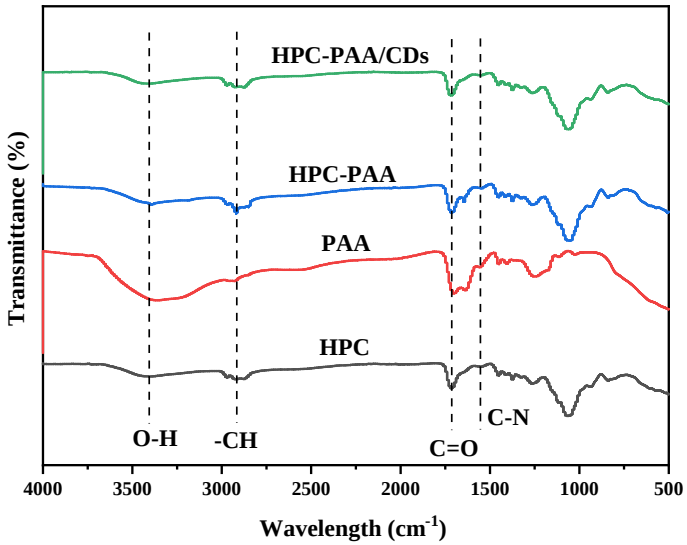


**Figure 3** FTIR spectra of the HPC hydrogel, PAA, HPC-PAA composite hydrogel sample, and HPC-PAA/CDs composite hydrogel sample.

hydrogel turned into hydrophobic dominant, so that the polymer was separated from water, and the pore size became significantly smaller (Figure 2E). With the incorporation of CDs, the microstructure of the hydrogel did not change and still maintained a 3D network structure, as shown in Figure 2C and F. The pores of the hydrogel became smaller after the phase transition at a higher temperature, similar to the morphology of HPC-PAA hydrogel. This suggested that the existence of CDs would not affect the crosslinked microstructure of the composite hydrogel. As illustrated in Figure 2G, the CD particles were observed in the hydrogel matrix by even distribution, which was attributed to the hydrogen bonding interactions between

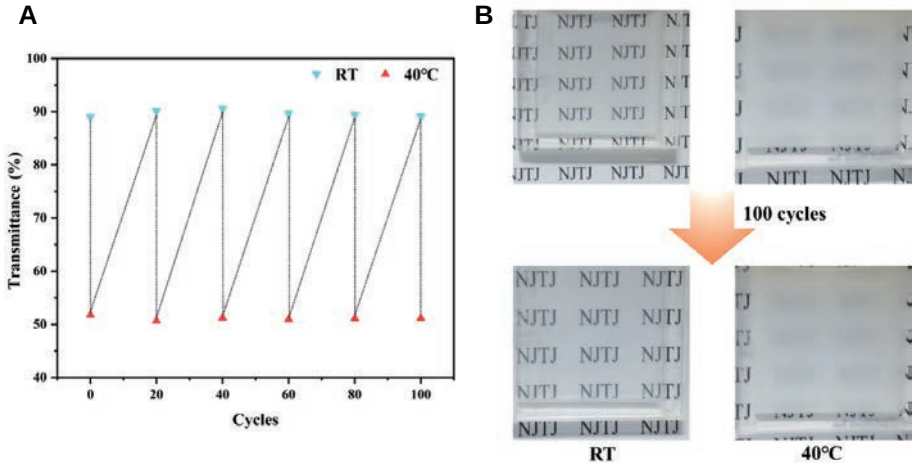


**Figure 4** (A) Luminous transmittance ($T_{vis}$) and (B) optical images of the HPC-PAA/CD composite hydrogel smart window sample at RT and 40°C before and after 100 phase transition cycles.

CDs and polymer chains, impeding the agglomeration of the CD particles and thus providing enhanced photothermal conversion efficiency. The common particle size of the CDs was observed to be less than 5 nm from measurement in the TEM image, which was consistent with the raw CD material.

In Figure 3, the FTIR spectra of HPC, PAA, HPC-PAA, and HPC-PAA/CDs were illustrated and compared. It was shown that the spectrum of the HPC-PAA sample contained the characteristic peaks of HPC and PAA materials. The –OH stretching vibration was observed at 3300–3600 $cm^{-1}$, and characteristic peaks at 2900, 1710, and 1550 $cm^{-1}$ were ascribed to C–H, C=O, and C–N groups, respectively. This was because the –CH of HPC and –COOH of PAA were mainly connected by hydrogen bonds and did not change the functional group structure. With the increase of temperature, the –OH group of HPC and the –COOH group of PAA chain, as well as the –OH group of HPC and water molecules, formed a competitive relationship between hydrogen bonding force and resulted in the decreased pore size in HPC-PAA composite hydrogel powder sample. In an acidic environment, high concentrations of $H^+$ in solution can promote hydrogen bonding and reduce the LCST of HPC-PAA composite hydrogels. Under neutral or alkaline conditions, the LCST of HPC-PAA composite hydrogels did not show noticebale change due to the low activity of $H^+$, which limited the formation of hydrogen bonds. In addition, the addition of CDs did not change the original functional group structure of hydrogels, and the characteristic peaks of HPC-PAA/CDs hydrogels and HPC-PAA hydrogels were almost the same, supporting that the CDs and hydrogel interacted with each other in the way of hydrogen bonding instead of chemical bonding. The doped CDs were used to accelerate the photothermal conversion rate in the hydrogel.

Previous studies presented that the HPC and HPC-based hydrogels possess the advantages of good durability with high stability and recyclability [50,51]. It has shown that the solar modulation capability of such a hydrogel-based smart window remained constant under exposure to UV light for 10 days [28]. In this work, the HPC-PAA/CDs composite hydrogel smart window sample with pH 2.6 has been conducted for cyclic stability test. As can be seen from Figure 4A and B, the visible light transmittance ($T_{vis}$) of the smart window remained basically unchanged after 100 cycles at RT and 40°C. The optical image of the smart window remained highly transparent at RT and appeared opaque at 40°C. These phenomena showed that the HPC-

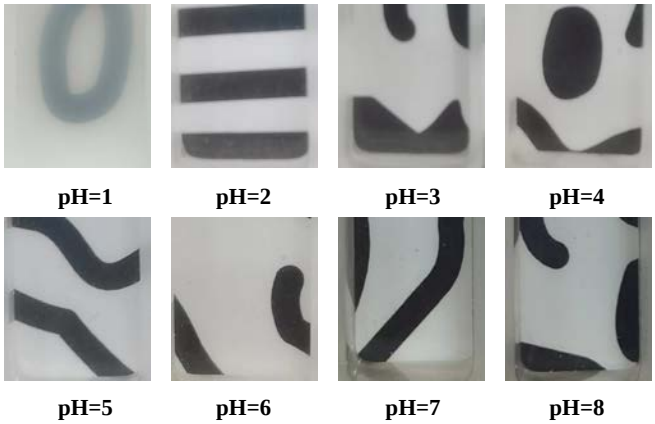


**Figure 5** Optical images of HPC-PAA composite hydrogels under different pH levels at 30°C.

PAA/CDs composite hydrogel smart window has excellent and stable reversible light conversion performance and solar modulation ability.

## Optical-thermal properties of HPC-PAA and HPC-PAA/CDs composite hydrogel

Figure 5 shows the optical images of HPC-PAA composite hydrogel samples at different pH values under 30°C. It can be found that the transparency of HPC-PAA composite hydrogel increases with the increase in pH level, and when the pH value is less than 3, the hydrogel is translucent. This is because under an acidic condition, PAA groups lose part of their negative charge and change the internal electrical properties of HPC-PAA composite hydrogels, thus promoting the cross-linking and gelation of PAA. With the continuous increase of pH value, the PAA group will attract a large amount of water and form a negative charge, thereby reducing the ion crosslinking inside the HPC-PAA composite hydrogel, making the hydrogel molecules unravel, losing their gel properties, and become colorless and transparent. Figure 6A shows the tunable LCSTs of the HPC-PAA composite hydrogel at 580 nm. It was also found that the transmittance of the hydrogel decreases with increasing temperature at all pH conditions. The LCST of the hydrogel increased from 11°C at pH 1 to 32°C at pH 3, and then remained almost constant once the pH level got greater than 7. As such, the LCST of the HPC-PAA/CDs composite hydrogel can be tuned by adjusting the pH level to meet the energy efficiency requirements of a smart window in different locations, seasons, and climates.

Figure 6C–F quantitatively present the solar transmittance spectra of hydrogels before and after phase transition for the samples with different LCSTs for solar light band of 250–2500 nm. As the temperature increases, the solar transmittance decreases nearly in the whole wavelength range, and the transmittance of hydrogels before and after the phase transition varies greatly. Generally, when the temperature is lower than LCST, the hydrogel has a very high transparency in the visible range. It can be seen that the pH level can influence the sunlight modulation ability of the hydrogel significantly. The light modulation became intensive when the pH value decreased from 3 to 1, and this was barely discussed by material scientists in smart windows. The solar modulation capability of hydrogel-based smart window may be further improved by controlling the pH value of the system on this basis. However, changing the pH level of the hydrogel to dynamically control the LCST is quite difficult in practical building applications because of possibly in-

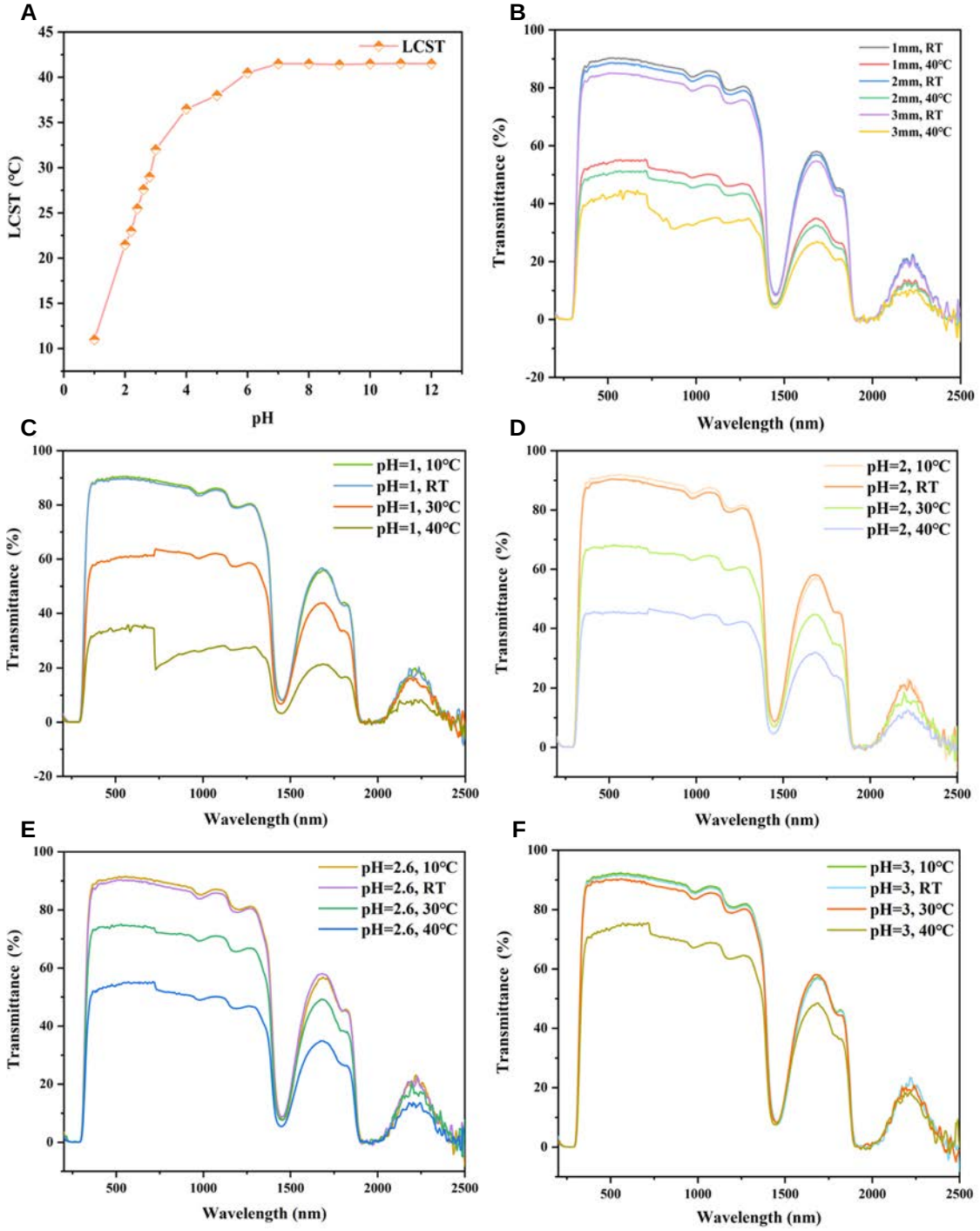


**Figure 6** (A) Phase transition temperatures of HPC-PAA composite hydrogel under different pH levels; (B) UV-Vis-NIR transmission spectra of HPC-PAA/CDs composite hydrogel smart windows with pH 2.6 at 20 and 40°C at different thicknesses; solar transmittance spectra of HPC-PAA/CDs composite hydrogel smart windows with pHs of (C) 1, (D) 2, (E) 2.6, and (F) 3, respectively.

creasing fenestration system complexity, operational costs, and safety issues to occupants and environments. Further research needs to be conducted to obtain the capability of pH regulating in gel, which may be induced by light radiation [52] or electricity [53,54]. It is clearly observed from the spectra in Figure 6C–F that the

**Table 1** Transmittance of HPC-PAA/CDs composite hydrogels of different thicknesses at RT and 40°C in different wavelength regions

| | Thickness and temperature | | | | | |
|---|---|---|---|---|---|---|
| | 1 mm, RT | 2 mm, RT | 3 mm, RT | 1 mm, 40°C | 2 mm, 40°C | 3 mm, 40°C |
| $T_{lum}$ (%) | 90.97 | 88.45 | 84.91 | 54.71 | 50.88 | 43.04 |
| $T_{NIR}$ (%) | 30.41 | 29.67 | 28.49 | 17.76 | 14.62 | 12.24 |
| $T_{sol}$ (%) | 82.35 | 80.12 | 76.91 | 48.79 | 45.37 | 36.39 |

**Table 2** $\Delta T_{lum}$, $\Delta T_{NIR}$, and $\Delta T_{sol}$ of HPC-PAA/CDs composite hydrogel smart windows of different thicknesses

| | Thickness | | |
|---|---|---|---|
| | 1 mm | 2 mm | 3 mm |
| $\Delta T_{lum}$ (%) | 36.26 | 37.57 | 41.87 |
| $\Delta T_{NIR}$ (%) | 12.65 | 15.05 | 16.25 |
| $\Delta T_{sol}$ (%) | 33.56 | 34.75 | 40.52 |

modulation property of the hydrogel material is relatively weak in NIR region compared with that of the visible light region, especially for the wavelengths of 1500 to 2500 nm. This is consistent with related studies [28,55], and shows that pure hydrogel in smart window applications is more suitable to regulate visible lights and limited NIR lights. Our recent studies [23,56] revealed that the poor NIR regulation ability of the hydrogels can be effectively improved by fabricating a large particle size of microgel whose dimensionless size parameter reaches unity in the NIR region, with a high $\Delta T_{NIR}$ of 76%.

The thickness of the HPC-PAA/CDs composite hydrogel has a dramatic influence on the optical properties of the smart window samples. Figure 6B shows the UV-Vis-NIR transmission spectra of the smart window with different thicknesses. Tables 1 and 2 display the thickness-related illuminance transmittance ($T_{lum}$), $T_{NIR}$, $T_{sol}$, $\Delta T_{lum}$, $\Delta T_{NIR}$, and $\Delta T_{sol}$. The overall transmittance of the sample decreases with the increase in the thickness of the hydrogel sample from 1 to 3 mm. Meanwhile, the values of $\Delta T_{lum}$, $\Delta T_{NIR}$, and $\Delta T_{sol}$ increase by 5.61%, 3.6%, and 6.69%, respectively, as the hydrogel thickness increases from 1 to 3 mm, suggesting that the hydrogel sample has better solar modulation ability with compensation of a slightly lower light transmission value.

## Enhanced thermal response of the hydrogel

Figure 7A shows the light transmittance of HPC-PAA/CDs composite hydrogel at room temperature. It can be observed that the addition of CDs barely reduces the light transmittance of HPC-PAA composite hydrogel, and the luminous transmittance is still at a high level of ~90%, indicating that the incorporation of CDs would not influence the optical properties of the hydrogel sample nor affect the natural lighting performance of the smart window when LCST is not reached. As an example, when the mass ratio of CDs and HPC is 1:100, the $T_{lum}$ of the smart window is 89.73%. Moreover, as shown in Table 3, the light transmittance including $T_{lum}$, $T_{NIR}$, and $T_{sol}$ of the HPC-PAA/CD samples under different CD addition amounts are close, further supporting that there is little influence of CDs on the adaptive solar modulation performance of the hydrogel sample.

The effect of different CD addition amounts on the thermochromic rate of hydrogel is presented in Figure 7C. All the samples were placed over the graphene-based heating plate to achieve a uniform heating

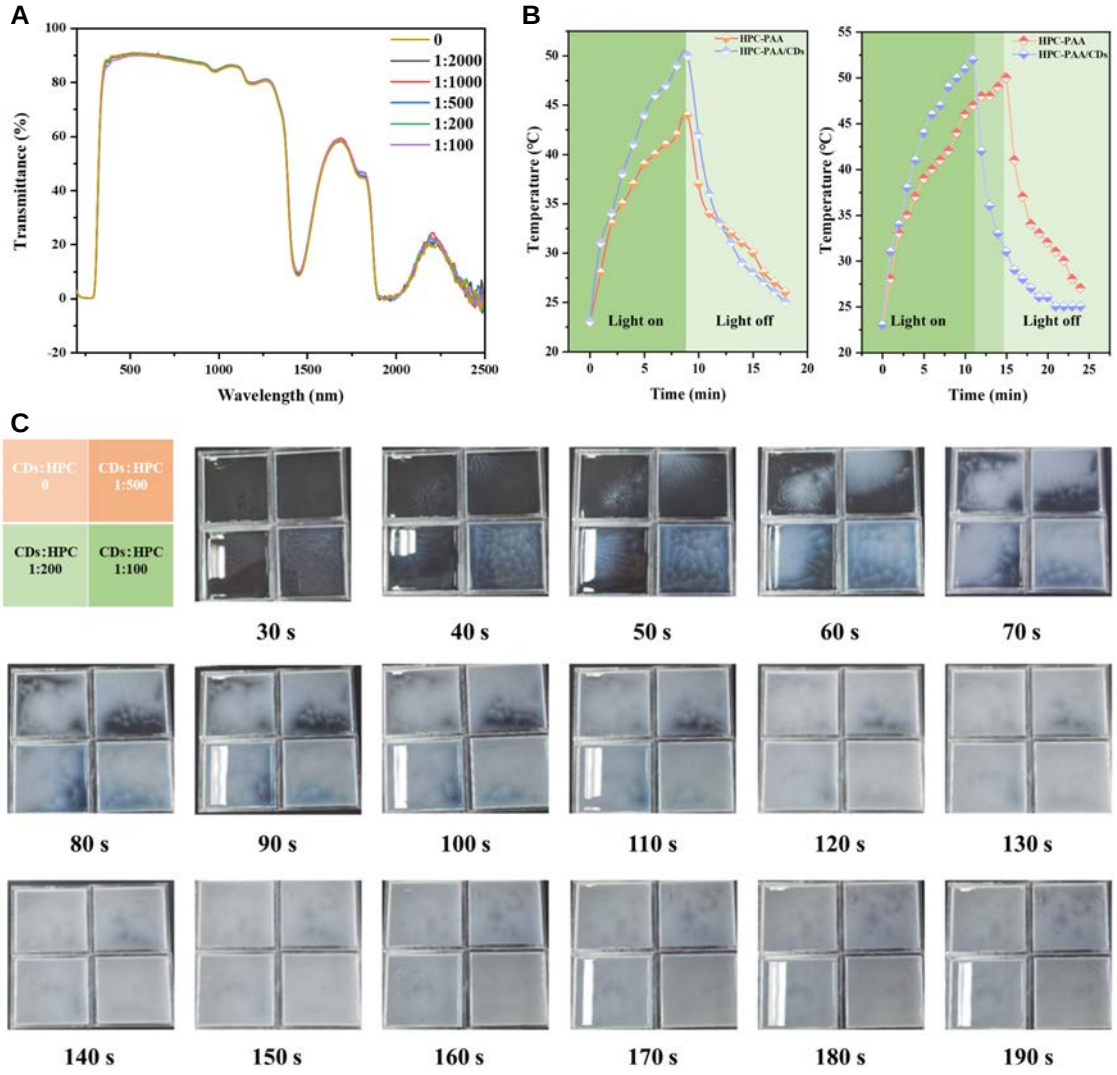


**Figure 7** (A) Light transmittance of HPC-PAA/CDs composite hydrogels with different ratios of CDs and HPC addition; (B) the rising and cooling rate plots of HPC-PAA composite hydrogel and HPC-PAA/CDs composite hydrogel with a 1:100 ratio of CDs to HPC addition; (C) phase transition rate diagram of HPC-PAA/CDs composite hydrogels with different addition ratios of CDs and HPC.

**Table 3** The light transmittance of HPC-PAA/CDs composite hydrogels with different CDs and HPC addition ratios in different wavelength regions

| CDs:HPC | 0 | 1:2000 | 1:1000 | 1:500 | 1:200 | 1:100 |
|---|---|---|---|---|---|---|
| $T_{lum}$ (%) | 90.97 | 90.61 | 90.46 | 90.41 | 90.25 | 89.73 |
| $T_{NIR}$ (%) | 30.41 | 30.51 | 30.46 | 30.36 | 30.28 | 30.33 |
| $T_{sol}$ (%) | 82.35 | 82.23 | 82.04 | 81.93 | 81.75 | 81.45 |

condition. The temperature of the heating plate was kept at 45°C, and after heating of 30 s, the hydrogel with the highest added CDs began to undergo a phase transition, and white cloudy polymers precipitated out of the liquid, showing a fast heat transfer setting. After heating for 120 s, the hydrogel with a CDs/HPC ratio of 1:100 was completely opaque; that is, the phase transition process was complete. These results indicated that

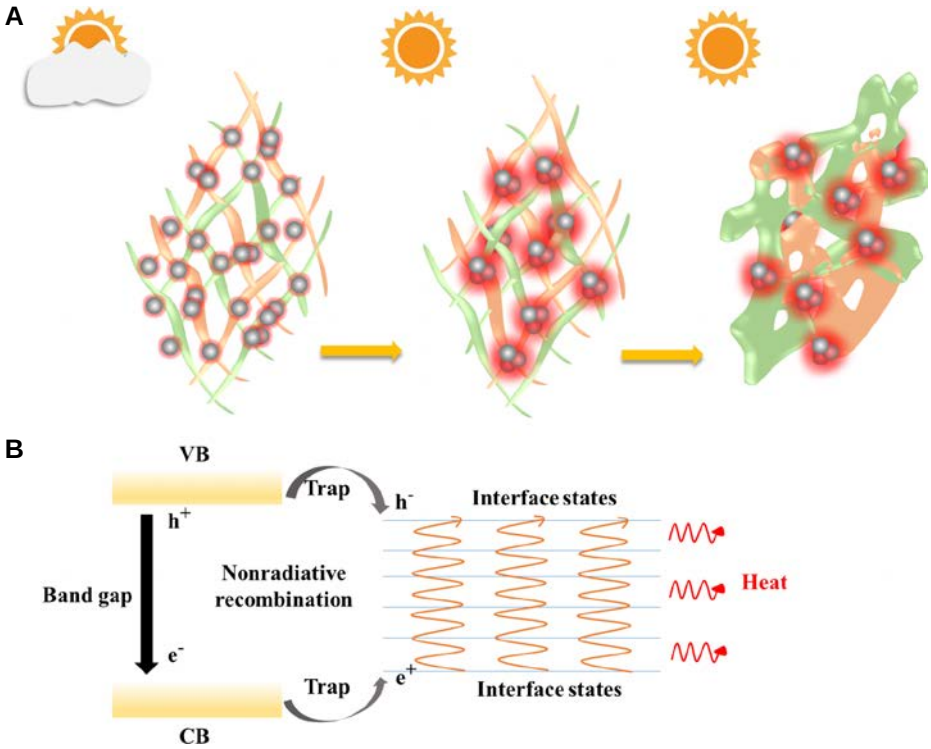


**Figure 8** (A) Schematic diagram of the working mechanism of CDs in the hydrogel system; (B) photothermal conversion mechanism of CDs under radiation.

the CDs can accelerate the thermochromism rate of HPC-PAA/CDs composite hydrogels. Once stopping the heating, the hydrogel changed to a completely transparent form after 50 s, which was shorter than the time needed for the bare HPC-PAA hydrogel sample.

A xenon lamp was employed to simulate sunlight with a power of 1000 W. After radiating the smart window devices of the HPC-PAA and the HPC- PAA/CDs hydrogels with a CDs/HPC mass ratio of 1:100, temperature profiles of the smart window device were shown in Figure 7B. Obviously, the CD-added sample possessed a faster temperature-rising rate than the sample without CDs. After exposed to xenon lamp radiation for 9 min, the HPC-PAA/CDs hydrogel smart window was heated to 51°C; in the meanwhile, the temperature of the HPC-PAA smart window was just 44°C. At that time, the lamp was immediately turned off, and the hydrogel smart window device began to cool down. It can be found that the HPC-PAA/CDs hydrogel device cooled down faster from 51°C to 26°C in 8 min, and the HPC-PAA hydrogel smart window cooled down from 44°C to 27°C for a same period. It can also be observed in Figure 7B that in another experiment, the HPC-PAA/CDs sample reached 52°C in 11 min, but the HPC-PAA sample reached 50°C in 15 min. These results intuitively proved that the CDs possessed the ability to accelerate the rate of phase transition of hydrogels owing to the photothermal effect, seen in Figure 7C.

Contributed from quantum confinement in 0D scale, CDs have an outstanding absorption capability in the visible and NIR spectra under the radiation of sunlight, allowing them to effectively absorb energy and excite electrons on the surface to a high energy level, and thus micro-aggregated CDs occur. As illustrated in Figure 8, the heat generated by the micro-aggregated CDs through nonradiative recombination of photo-

**Table 4** Comparison of phase transition rates of electrochromic and thermochromic smart windows

| Stimuli | Type | Material | Switching speed (s) | Ref. |
|---|---|---|---|---|
| Electrochromic | Inorganic metal oxides | $WO_3$ | 7.28, 2.64 | [60] |
| | | $WO_3$ | 12, 5 | [61] |
| | | NiO@C | 11.5, 9.5 | [62] |
| | | $W_{18}O_{49}$ HMP | 8.6, 7 | [63] |
| | Organic polymers | DAT-DMP | <5 | [64] |
| | | PANI | 5.9, 16.9 | [65] |
| | | PA-ECD | 17.6, 28.5 | [66] |
| | Liquid | DDCLC with CB7CB | 0.117 | [67] |
| | | DDCLC | 1.22 | [68] |
| | | 5CB-based supramolecular LC | 0.2 | [69] |
| Thermochromic | $VO_2$ | W-doped $VO_2$/starch derivative hybrid | 300 | [70] |
| | | $VO_2$-$W_{18}O_{49}$ composite film | 174 | [71] |
| | Liquid | IDI-LC | 120 | [72] |
| | | CNT-PDB | 1.2 | [73] |
| | Hydrogel | pNIPAm−AEMA microgels | 300 | [56] |
| | | HPC/PAA hydrogel | 84 | [30] |
| | | PHC-Gel | 10.6 | [74] |
| | | HPC-PAA/CDs hydrogel | 30 | This work |

excited charge carriers diffuses locally to the hydrogel network attached with CDs by interfacial interaction, and promotes the phase transition of the hydrogel. In addition, CDs also interact with the structure of the hydrogel network, enhancing light absorption and shortening the distance between CDs anchored on the hydrogel network, thus forming larger CD aggregates and greatly promoting the photothermal conversion rate of CDs. Besides, it was reported that the interaction between CDs and polymer networks would alter the electronic structure and change the behavior of photoexcited charge carriers of CDs, thus further improving the light-to-heat conversion efficiency [57]. The above phenomenon explains the fact that the incorporation of CDs could effectively enhance the thermochromic switching speed of the hydrogel. Previous studies have shown that carbon-based materials can increase the thermal conductivity of phase change materials (PCM) [58,59]. Table 4 summarizes the transformation speeds of the two categories of smart windows. The phase transition time of electrochromic smart window is usually less than 30 s, while the phase transition time of thermochromic smart window is generally far long, as much as about 5 min. As such, in this work, a post deposition method with the addition of CDs was proposed to shorten the phase transition time of hydrogel dramatically, which could be beneficial to building energy-saving performance and human visual comfort.

## Building energy performance simulation

To explore the effect of tunable phase transition temperature of hydrogel-based smart window on building energy performance, a whole building energy simulation was carried out using EnergyPlus [75,76]. A typical single-room building with a floor dimension of 20 m × 10 m × 4 m ($L \times W \times H$) was employed as the prototype building in the simulation, as shown in Figure 9F. The building wall and roof insulations meet the minimum requirements specified in ASHRAE building codes for nonresidential buildings (e.g., above-grade steel frame walls and insulation entirely above deck for roofs). The roof was made of roof membrane, roof

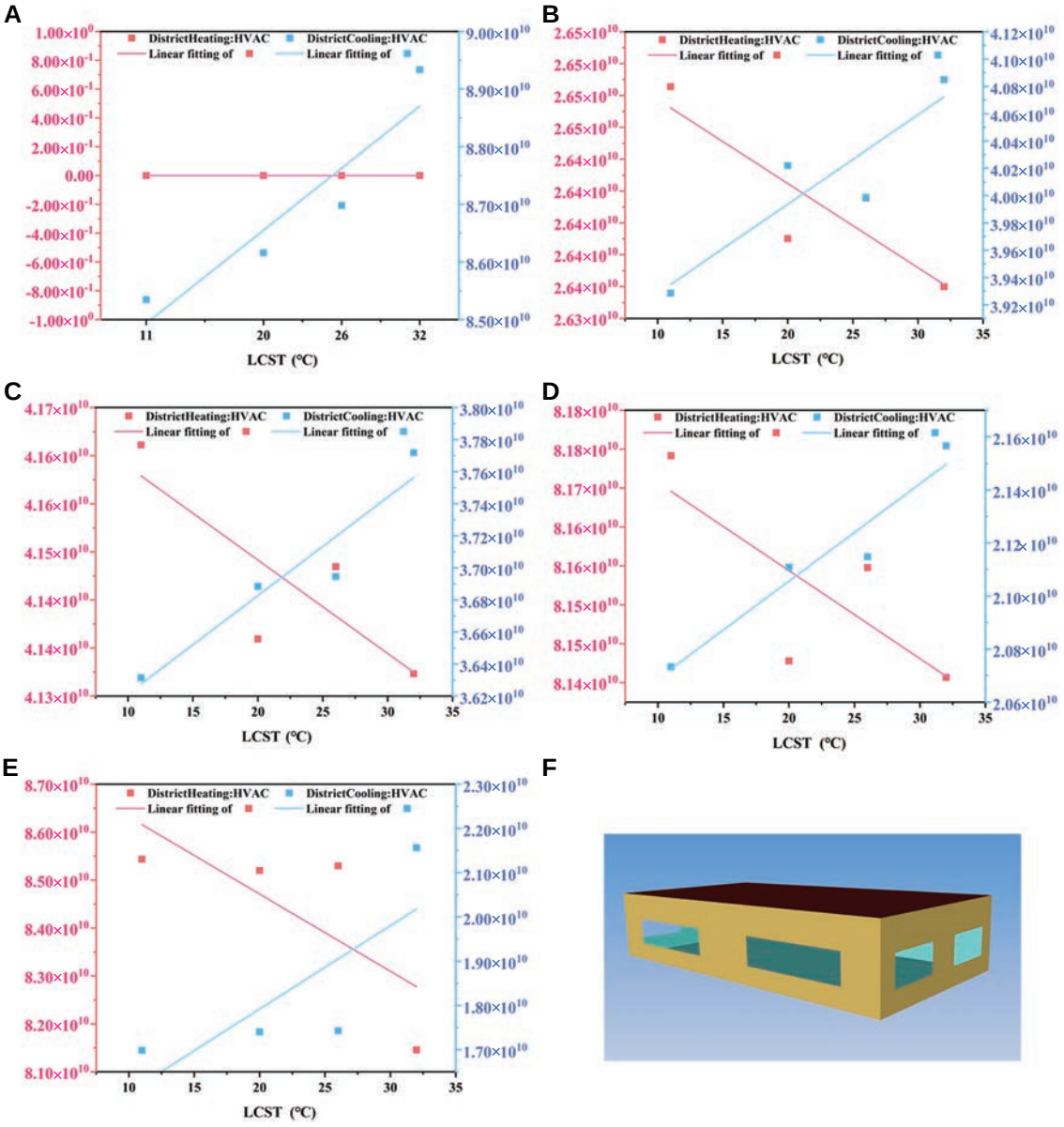


**Figure 9** Annual heating and cooling energy consumption profiles (Joule) for (A) Singapore, (B) Nanjing, (C) Beijing, (D) Moscow, and (E) Helsinki; (F) geometrical model of the prototype building.

insulation, and metal decking. The heating and cooling energy demands were modeled by applying "ideal-loads-air-systems" served with district cooling and heating sources. The heating and cooling energy consumptions were evaluated by applying the site-to-source energy conversion factors of 1.28 and 1.05 for district heating and cooling, respectively. The internal gains of the constructed model included occupants (0.06 person/$m^2$), lights (a power of 10.7 W/$m^2$) and electric equipment (a power of 5.8 W/$m^2$). To represent the direct effects of cooling/heating energy consumption on tunable LCST properties of smart window, the prototype model and calculation algorism were simplified, and the daylighting demands were not counted. Five typical locations ranging from tropical region to cold region, including Singapore, Nanjing, Beijing,

Moscow, and Helsinki, were selected for simulation, corresponding to ASHRAE climate zones 1, 3, 4, 6, and 7, respectively.

Figure 9A–E present the annual heating and cooling energy consumptions of the prototype building installed with hydrogel smart windows in the selected locations, showing the impact of the tunable LCST on the building energy under various climates. The dots in Figure 9 represent the annual energy consumption for heating and cooling for the selected cities, and the lines were plotted to demonstrate the increasing and decreasing trends for the annual energy consumption as a function of different LCST values. The lines are beneficial to intuitively observe the influence of phase change temperature on energy consumption so as to effectively study the impact of phase change temperature on the annual heating and cooling energy. The increase of LCST from 11°C to 32°C would lead to a reduction of the heating energy consumption, accompanying with increase in the cooling energy consumption in the modeled building. It is clear to observe that the transition temperature of the smart window, ranging from 11°C to 32°C, had a significant impact on building cooling energy, compared with heating energy. Considering that the window-to-wall ratio of the proposed model house was 40%, typical commercial buildings with curtain walls will get an even greater effect on the cooling and heating energy consumption and saving if applied with the tunable thermochromic hydrogel-based smart windows.

Figure 10 describes the monthly total cooling and heating energy consumption of the model house when employed with the LCST-tunable hydrogel smart widows. The lowest total energy consumption for cooling-dominated locations such as Singapore was achieved when the LCST was adjusted to a minimum value of 11°C. On the contrary, in cold climates such as Beijing, Moscow, and Helsinki, the modeled house requires more heating energy and shows the necessary need for a tunable LCST in order to achieve lower energy consumption. For example, in Moscow, a higher LCST is required in winter season, and the optimized LCST for January, February, March, October, November, and December is 20°C. On the other hand, a lower LSCT is required in summer season and the optimized LCST for April to September is 11°C. Despite regulating the solar transmittance of the thermochromic smart window benefits building energy efficiency, which has been widely investigated in recent years, this study proves that tunable phase transition temperature of thermochromic smart window will further improve the building energy performance. This dynamic feature also enables the smart window to be more weather adaptive and better suitable to diverse operational requirements. However, it should be noted that the optimized tunable LCST for different months under various climates could be lower than the required LCST in an actually operated building because the simulation did not include daylighting analysis.

## DISCUSSION

This work successfully prepared a type of cellulose-derived hydrogel film with tunable thermochromic and pH-sensitive features for smart window application. The characteristic analysis, including SEM microscopy and FTIR spectra, demonstrated that the HPC, PAA, and CDs were interacted through a strong hydrogen bonding force, where the CDs performed as active sites for photothermal conversion effects. The freeze-dried hydrogel sample showed a porous 3D structure. Before phase transition, the pure HPC hydrogel polymer was in flaky shape, whereas the HPC-PAA hydrogel polymer was needle-like, which was attributed to the

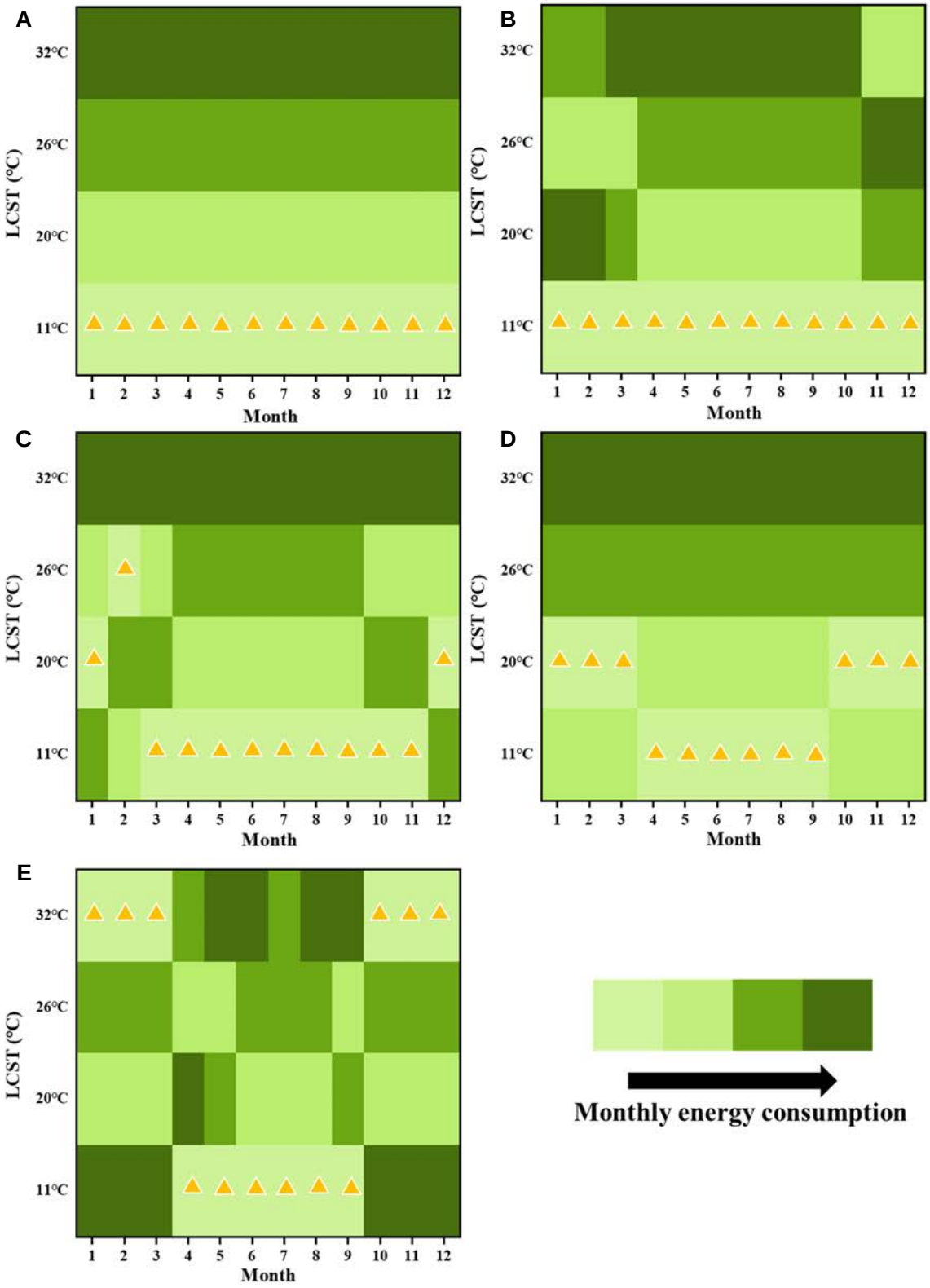


**Figure 10** Mapping for total building energy consumption for (A) Singapore, (B) Nanjing, (C) Beijing, (D) Moscow, and (E) Helsinki.

interaction between HPC and PAA groups. The swollen chains in both hydrogels tended to form granules by shrinkage. While the hydrogel sample maintained good solar regulation property and a comparable large $\Delta T_{sol}$ before and after phase transition, its LCST was tuned between 11 and 32°C by changing the pH level in the hydrogel solution, giving weather adaptive and flexible features for suitability to broad climates and locations. Moreover, the incorporation of CDs with the superior capability of photothermal conversion to the HPC-PAA composite hydrogel can significantly reduce the phase transition time and increase the response speed to the external stimulus. The heating-cooling cycle test demonstrated that the HPC-PAA/CDs smart window can quickly transfer to an opaque state within 80 s and block more lights from transmitting into a building as the hydrogel temperature reaches over LCST. Using a single-room building model and EnergyPlus tool, the whole building energy simulation has shown that the tunable LCST feature introduced different monthly and annual cooling and heating energy consumptions for the modeled five locations as well as climates. In particular, the locations with significant heating demand highly require LCST-tunable thermochromic smart windows while the locations dominated by cooling demand generally require low LCST if the lighting analysis was not included in consideration. This study provides insights into the design and development of adaptive building envelope and points out the importance and a new direction of tunability for smart building materials.

## Data availability

The original data are available from corresponding authors upon reasonable request.

## Funding

This work was supported by the National Key Research and Development Program of China (2023YFC3806300), and the Postgraduate Research & Practice Innovation Program of Jiangsu Province (KYCX23_1485).

## Author contributions

G.T. and T.J. proposed, designed, and guided the work. S.Z. performed the experiments and drafted the manuscript. S.Z., Y.X., G.T. and T.J. revised the manuscript. S.Z., Y.X. and H.L. contributed to the optical property analysis. K.W. contributed to the material fabrication. S.Z. and T.J. conducted the building energy simulation and analysis. Y.L., Z.P., G.T. and T.J. discussed the manuscript. All authors checked the manuscript.

## Conflict of interest

The authors declare no conflict of interest.

## References

1 Tanabe SI, Meliță L, Croitoru C, *et al*. Aerogel, a high performance material for thermal insulation: A brief overview of the building applications. *E3S Web of Conferences* 2019; **111**: 06069.

2 Fu Q, Han Z, Chen J, *et al.* Applications of reinforcement learning for building energy efficiency control: A review. *J Building Eng* 2022; **50**: 104165.

3 Lamy-Mendes A, Pontinha ADR, Alves P, *et al.* Progress in silica aerogel-containing materials for buildings' thermal insulation. *Construction Building Mater* 2021; **286**: 122815.

4 Amber KP, Ahmad R, Aslam MW, *et al.* Intelligent techniques for forecasting electricity consumption of buildings. *Energy* 2018; **157**: 886–893.

5 Zhang SC, Yang XY, Xu W, *et al.* Contribution of nearly-zero energy buildings standards enforcement to achieve carbon neutral in urban area by 2060. *Adv Clim Change Res* 2021; **12**: 734–743.

6 Jiang HD, Xue MM, Liang QM, *et al.* How do demand-side policies contribute to the electrification and decarburization of private transportation in China? A CGE-based analysis. *Tech Forecasting Soc Change* 2022; **175**: 121322.

7 Najjar MK, Figueiredo K, Hammad AWA, *et al.* A framework to estimate heat energy loss in building operation. *J Clean Prod* 2019; **235**: 789–800.

8 Long L, Ye H. How to be smart and energy efficient: A general discussion on thermochromic windows. *Sci Rep* 2014; **4**: 6427.

9 Chidubem Iluyemi D, Nundy S, Shaik S, *et al.* Building energy analysis using EC and PDLC based smart switchable window in Oman. *Sol Energy* 2022; **237**: 301–312.

10 Zhang S, Hu W, Li D, *et al.* Energy efficiency optimization of PCM and aerogel-filled multiple glazing windows. *Energy* 2021; **222**: 119916.

11 Buratti C, Belloni E, Merli F, *et al.* Aerogel glazing systems for building applications: A review. *Energy Build* 2021; **231**: 110587.

12 Ke Y, Chen J, Lin G, *et al.* Smart windows: Electro-, thermo-, mechano-, photochromics, and beyond. *Adv Energy Mater* 2019; **9**: 1902066.

13 Feng M, Bu X, Yang J, *et al.* Review: smart windows based on photonic crystals. *J Mater Sci* 2020; **55**: 8444–8463.

14 Zhu J, Huang A, Ma H, *et al.* Composite film of vanadium dioxide nanoparticles and ionic liquid-nickel-chlorine complexes with excellent visible thermochromic performance. *ACS Appl Mater Interfaces* 2016; **8**: 29742–29748.

15 Hakami A, Srinivasan SS, Biswas PK, *et al.* Review on thermochromic materials: Development, characterization, and applications. *J Coat Technol Res* 2022; **19**: 377–402.

16 Liu Y, Han Y, Huang Z, *et al.* New focus of the cloud point/Krafft point of nonionic/cationic surfactants as thermochromic materials for smart windows. *Chem Commun* 2022; **58**: 2814–2817.

17 Xu F, Cao X, Luo H, *et al.* Recent advances in $VO_2$-based thermochromic composites for smart windows. *J Mater Chem C* 2018; **6**: 1903–1919.

18 Gao Y, Luo H, Zhang Z, *et al.* Nanoceramic $VO_2$ thermochromic smart glass: A review on progress in solution processing. *Nano Energy* 2012; **1**: 221–246.

19 Feng YQ, Lv ML, Yang M, *et al.* Application of new energy thermochromic composite thermosensitive materials of smart windows in recent years. *Molecules* 2022; **27**: 1638.

20 Zhao Y, Ji H, Lu M, *et al.* Thermochromic smart windows assisted by photothermal nanomaterials. *Nanomaterials* 2022; **12**: 3865.

21 Wu L, Yu Q, Wang S, *et al.* Synthesis of dual cross-linked ion conductive temperature-sensitive hydrogel and its application in tunable smart window. *J Mater Sci* 2022; **57**: 12672–12684.

22 Tan Y, Zhang Y, Zhang Y, *et al.* Dual cross-linked ion-based temperature-responsive conductive hydrogels with multiple sensors and steady electrocardiogram monitoring. *Chem Mater* 2020; **32**: 7670–7678.

23 Jiang T, Zhao X, Yin X, *et al.* Dynamically adaptive window design with thermo-responsive hydrogel for energy efficiency. *Appl Energy* 2021; **287**: 116573.

24 Vanti G, Wang M, Bergonzi MC, *et al.* Hydroxypropyl methylcellulose hydrogel of berberine chloride-loaded escinosomes: Dermal absorption and biocompatibility. *Int J Biol Macromol* 2020; **164**: 232–241.

25 Martin-Pastor M, Stoyanov E. Mechanism of interaction between hydroxypropyl cellulose and water in aqueous solutions: Importance of polymer chain length. *J Polym Sci* 2020; **58**: 1632–1641.

26 Allen K, Connelly K, Rutherford P, *et al.* Smart windows—Dynamic control of building energy performance. *Energy Build* 2017; **139**: 535–546.

27 Chen Y, Ding D, Mao Z, *et al.* Synthesis of hydroxypropylcellulose-poly(acrylic acid) particles with semi-interpenetrating polymer network structure. *Biomacromolecules* 2008; **9**: 2609–2614.

28 Yang YS, Zhou Y, Yin Chiang FB, *et al.* Temperature-responsive hydroxypropylcellulose based thermochromic material

and its smart window application. *RSC Adv* 2016; **6**: 61449–61453.

29 Yao R, Xu J, Lu X, *et al.* Phase transition behavior of HPMC-AA and preparation of HPMC-PAA nanogels. *J Nanomaterials* 2011; **2011**: 1–6.

30 Zhang L, Xia H, Xia F, *et al.* Energy-saving smart windows with HPC/PAA hybrid hydrogels as thermochromic materials. *ACS Appl Energy Mater* 2021; **4**: 9783–9791.

31 Liao Q, Shao Q, Wang H, *et al.* Hydroxypropylcellulose templated synthesis of surfactant-free poly(acrylic acid) nanogels in aqueous media. *Carbohyd Polym* 2012; **87**: 2648–2654.

32 Liao Q, Shao Q, Qiu G, *et al.* Methacrylic acid-triggered phase transition behavior of thermosensitive hydroxypropylcellulose. *Carbohyd Polym* 2012; **89**: 1301–1304.

33 Warwick MEA, Ridley I, Binions R. The effect of transition gradient in thermochromic glazing systems. *Energy Build* 2014; **77**: 80–90.

34 Cao D, Xu C, Lu W, *et al.* Sunlight-driven photo-thermochromic smart windows. *Sol RRL* 2018; **2**: 1700219.

35 Zhu H, Wang L. Smart window based on $Cu_7S_4$/hydrogel composites with fast photothermal response. *Sol Energy Mater Sol Cells* 2019; **202**: 110109.

36 Kim HJ, Kim B, Auh Y, *et al.* Conjugated organic photothermal films for spatiotemporal thermal engineering. *Adv Mater* 2021; **33**: 2005940.

37 Sun S, Chen Q, Li Y, *et al.* Tumor-specific and photothermal-augmented chemodynamic therapy by ferrocene-carbon dot-crosslinked nanoparticles. *SmartMat* 2022; **3**: 311–322.

38 Meng X, Qiao J, Yang Y, *et al.* Three-dimensional porous manganese oxide/nickel/carbon microspheres as high-performance electromagnetic wave absorbers with superb photothermal property. *J Colloid Interface Sci* 2023; **629**: 884–894.

39 Chen T, Yao T, Peng H, *et al.* An injectable hydrogel for simultaneous photothermal therapy and photodynamic therapy with ultrahigh efficiency based on carbon dots and modified cellulose nanocrystals. *Adv Funct Mater* 2021; **31**: 2106079.

40 Chao W, Li Y, Sun X, *et al.* Enhanced wood-derived photothermal evaporation system by *in-situ* incorporated lignin carbon quantum dots. *Chem Eng J* 2021; **405**: 126703.

41 Zheng Z, Li H, Zhang X, *et al.* High-absorption solar steam device comprising Au@$Bi_2MoO_6$-CDs: Extraordinary desalination and electricity generation. *Nano Energy* 2020; **68**: 104298.

42 Roy A, Manna K, Dey S, *et al.* Chemical modification of β-cyclodextrin towards hydrogel formation. *Carbohyd Polym* 2023; **306**: 120576.

43 Wang M, Xia A, Wu S, *et al.* Facile synthesis of the Cu, n-CDs@GO-CS hydrogel with enhanced antibacterial activity for effective treatment of wound infection. *Langmuir* 2021; **37**: 7928–7935.

44 Chen H, Ma X, Wu S, *et al.* A rapidly self-healing supramolecular polymer hydrogel with photostimulated room-temperature phosphorescence responsiveness. *Angew Chem Int Ed* 2014; **53**: 14149–14152.

45 Bastos Porsani G, Casquero-Modrego N, Echeverria Trueba JB, *et al.* Empirical evaluation of EnergyPlus infiltration model for a case study in a high-rise residential building. *Energy Build* 2023; **296**: 113322.

46 Yoo W, Clayton MJ, Yan W. ESMUST: EnergyPlus-driven surrogate model for urban surface temperature prediction. *Build Environ* 2023; **229**: 109935.

47 Bastos Porsani G, Fernández Bandera C. A case study of empirical validation of energyplus infiltration models based on different wind data. *Buildings* 2023; **13**: 511.

48 Feng F, Fu Y, Yang Z, *et al.* Enhancement of phase change material hysteresis model: A case study of modeling building envelope in EnergyPlus. *Energy Build* 2022; **276**: 112511.

49 Varzandeh A, Sajadi B. Energy performance sensitivity analysis on building's passive technologies effective parameters, in an NZEB energyplus-simulated villa in Tehran's weather conditions with OFAT methods. *Energy Equipment Systems* 2023; doi: 10.22059/EES.2023.1986001.1416.

50 Zhang L, Du Y, Xia H, *et al.* HPC-PAA hydrogel smart windows with and without $Cs_{0.32}WO_3$: High solar modulation

ability and luminous transmittance. *Ceramics Int* 2022; **48**: 37122–37131.

51 Guo Y, Guan W, Lei C, *et al.* Scalable super hygroscopic polymer films for sustainable moisture harvesting in arid environments. *Nat Commun* 2022; **13**: 2761.

52 Wimberger L, Andréasson J, Beves JE. Basic-to-acidic reversible pH switching with a merocyanine photoacid. *Chem Commun* 2022; **58**: 5610–5613.

53 Yang G, Yu Y, Yang B, *et al.* A multiple chirality switching device for spatial light modulators. *Angew Chem Int Ed* 2020; **60**: 2018–2023.

54 Yang G, Yao Z, Yang X, *et al.* A flexible circularly polarized luminescence switching device based on proton-coupled electron transfer. *Adv Sci* 2022; **9**: e2202636.

55 Zhou Y, Cai Y, Hu X, *et al.* $VO_2$/hydrogel hybrid nanothermochromic material with ultra-high solar modulation and luminous transmission. *J Mater Chem A* 2015; **3**: 1121–1126.

56 Li XH, Liu C, Feng SP, *et al.* Broadband light management with thermochromic hydrogel microparticles for smart windows. *Joule* 2019; **3**: 290–302.

57 Chang Q, Shen Z, Guo Z, *et al.* Hydroxypropylmethyl cellulose modified with carbon dots exhibits light-responsive and reversible optical switching. *ACS Appl Mater Interfaces* 2021; **13**: 12375–12382.

58 Sarrafha H, Kasaeian A, Jahangir MH, *et al.* Transient thermal response of multi-walled carbon nanotube phase change materials in building walls. *Energy* 2021; **224**: 120120.

59 Chen X, Cheng P, Tang Z, *et al.* Carbon-based composite phase change materials for thermal energy storage, transfer, and conversion. *Adv Sci* 2021; **8**: 2001274.

60 Li Y, McMaster WA, Wei H, *et al.* Enhanced electrochromic properties of $WO_3$ nanotree-like structures synthesized via a two-step solvothermal process showing promise for electrochromic window application. *ACS Appl Nano Mater* 2018; **1**: 2552–2558.

61 Cheng W, He J, Dettelbach KE, *et al.* Photodeposited amorphous oxide films for electrochromic windows. *Chem* 2018; **4**: 821–832.

62 Liang H, Li R, Li C, *et al.* Regulation of carbon content in MOF-derived hierarchical-porous NiO@C films for high-performance electrochromism. *Mater Horiz* 2019; **6**: 571–579.

63 Xu S, Li X, Ou Y, *et al.* Ultra-large optical modulation of a size-tunable flexible electrochromic honeycomb mesoporous tungsten oxide film. *Inorg Chem Front* 2019; **6**: 680–686.

64 Christiansen DT, Reynolds JR. A fruitful usage of a dialkylthiophene comonomer for redox stable wide-gap cathodically coloring electrochromic polymers. *Macromolecules* 2018; **51**: 9250–9258.

65 Wang Q, Cao S, Meng Q, *et al.* Robust and stable dual-band electrochromic smart window with multicolor tunability. *Mater Horiz* 2023; **10**: 960–966.

66 Park C, Kim JM, Kim Y, *et al.* High-coloration efficiency and low-power consumption electrochromic film based on multifunctional conducting polymer for large scale smart windows. *ACS Appl Electron Mater* 2021; **3**: 4781–4792.

67 Lu H, Zhu M, Cao Y, *et al.* Fast-relaxation, dye-doped cholesteric liquid-crystal smart window with a perfect planar state. *Dyes Pigments* 2023; **208**: 110795.

68 Cheng WF, Lai JC, Fang Jie ST, *et al.* Scattering-/absorption-mode light shutters based on dye-doped fingerprint chiral textures. *Dyes Pigments* 2019; **163**: 78–85.

69 Li Y, Chen Y, Zhang J, *et al.* Dual electric/magnetic field-modulated nematic liquid crystal smart window based on the supramolecular doping effect of halloysite nanotube directors. *ACS Appl Nano Mater* 2023; **6**: 4532–4543.

70 Wang Y, Zhao F, Wang J, *et al.* Tungsten-doped $VO_2$/starch derivative hybrid nanothermochromic hydrogel for smart window. *Nanomaterials* 2019; **9**: 970.

71 Qian J, Li B, Tian S, *et al.* Near-infrared-activated $VO_2$ based nanothermochromic smart windows by incorporation of photothermal $W_{18}O_{49}$ nanorods. *Appl Surf Sci* 2022; **605**: 154680.

72 Meng W, Gao Y, Hu X, *et al.* Photothermal dual passively driven liquid crystal smart window. *ACS Appl Mater Interfaces* 2022; **14**: 28301–28309.

73 Deng Y, Li SQ, Yang Q, *et al.* High-efficiency responsive smart windows fabricated by carbon nanotubes modified by liquid crystalline polymers. *Crystals* 2021; **11**: 440.

74 Xie L, Wang X, Zou X, *et al.* Engineering self-adaptive multi-response thermochromic hydrogel for energy-saving smart windows and wearable temperature-sensing. *Small* 2023; **19**: 2304321.

75 Chuah JW, Raghunathan A, Jha NK. ROBESim: A retrofit-oriented building energy simulator based on EnergyPlus. *Energy Build* 2013; **66**: 88–103.

76 Lyons P, Wong J, Bhandari M. A comparison of window modeling methods in EnergyPlus 4.0. In: Fourth National Conference of IBPSA-USA. New York, 2010; 177–184.